**Original Research Article**

# Formulation of Anti-tuberculosis Drug Loaded Starch Propionate Microparticles for Controllable Drug Delivery


## ABSTRACT

The goal of this study was to use an emulsification solvent evaporation approach to formulate anti-tuberculosis drug (isoniazid, rifampicin, and pyrazinamide) loaded starch propionate microparticles (ATD-SPMPs). Fourier transform infrared spectrometry revealed that starch propionate (SP) exhibited new bands at 1749cm$^{-1}$ and 1236cm$^{-1}$, whereas SPMPs had identical peaks. The A-type pattern of native starch was entirely changed into the V-type pattern of SP by X-ray diffraction, while SPMPs showed a similar type pattern with SP having reduced crystallinity. Propionylation improved the thermal stability of native starch by reducing the number of hydroxyl groups in the modified starch molecule. SPMPs have superior thermal stability than SPMPs due to their semi-crystalline structure. In the optimized formulation, the highest percentage encapsulation efficiency of isoniazid, rifampicin, and pyrazinamide was determined to be 37.6%, 45.2%, and 43.1%, respectively. Scanning electron microscopy revealed that propionylation partially disturbed the granule morphology of native starches, and the imperfections and porosity structures of SP granules were completely changed into the uniform-sized spherical shape of SPMPs. The geometric particle sizes of the blank SPMPs, isoniazid, rifampicin, and pyrazinamide loaded SPMPs were 1.243 ± 0.3 μm, 1.65 ± 0.2 μm, 2.73 ± 0.7 μm, and 2.69 ± 0.5 μm, respectively. The dialysis bag method was used to study drug release from ATD-SPMPs and in-vitro drug release data was also analyzed using several kinetic models. The in-vitro drug release investigation revealed that drug release from SPMPs was controlled in comparison to pure ATD using the Korsmeyer-Peppas model, indicating drug release by anomalous diffusion, i.e., non-Fickian diffusion. Overall, the formulated ATD-SPMPs may be regarded as a potential anti-tuberculosis micro-drug, offers a path forward for tuberculosis clinics.



***Key Words:*** *Starch propionate, Anti-tuberculosis, Microparticles, Encapsulation, Drug release.*


## 1. INTRODUCTION

Infectious disease Mycobacterium tuberculosis is a chronic communicable disease that has infected billions of people worldwide. A quarter of the world's TB cases come from India, which is the second most populated country in the world [1]. The World Health Organization (WHO) estimates that 9.9 million people will be diagnosed with tuberculosis (TB) worldwide in 2020, with an estimated 1.3 million people dying from the disease [2]. Tuberculosis patients must take a considerable number of tablets, typically 9–16 per day for two months, followed by 3–9 per day for four to six months (continuation phase) in standard treatment. The rise of multidrug-resistant tuberculosis (MDR-TB) has highlighted the need for novel TB treatments. A lack of bioavailability and volatility in plasma drug concentrations limit the ability of conventional drug delivery devices to provide sustained release. Controlled drug delivery systems are being developed in an effort to address the issues associated with conventional drug delivery. Controlled drug delivery systems have evolved tremendously during the past two decades, ranging from micro and nanoscale to intelligent targeted delivery [4]. Sustained release

can be controlled by these micro- and nanoparticles as drug carriers, improving drug bioavailability indirectly and allowing for dose reduction and frequency reduction in addition to an improvement in patient compliance [5].

Isoniazid (INH), rifampicin (RIF), and pyrazinamide (PYZ) was the first-line antitubercular drug (ATD) used in "Category-III" tuberculosis treatment. Drug resistance, hepatotoxicity, nausea, rashes, and other side effects are common with these first-line ATD [6]. Toxicities, intolerance, and noncompliance with the whole treatment regimen might result from extended therapy and excessive doses of medicines. Treatment failure and recurrence are the most common outcomes. Incomplete management can potentially lead to drug resistance, necessitating the use of more harmful, more expensive, and less effective second- or third-line drugs [7]. There is a pressing need for new and effective anti-TB treatments to combat drug resistance, shorten the treatment period, and improve adherence. One of the advantages of micro- and nanoparticle based antituberculosis drugs over free drugs is that they may be regulated and sustained release, which is a major factor in micro and nanoparticle development. [8].

It is widely accepted that polymeric microparticles (MPs) are excellent transporters for lipophilic and hydrophilic drugs [9]. Particles of this type have several advantages, not the least of which being their ease of use and potential for industrial scale-up [10]. It is advisable to apply MPs to deliver drugs in a variety of ways, such as by encapsulating proteins and nucleic acids, or by administering the drugs via a variety of pathways. To utilize MPs for controlled drug release, one must choose a polymer and its chemical and molecular properties, such as molecular weight (MW), monomer composition, crystallinity, glass transition temperature (Tg), and inherent viscosity [13-16]. Many biodegradable polymers, such as alginate, dextran, chitosan, gelatin, and starch, can be utilized to fabricate MPs in this scenario [17–21]. It is preferable to employ these polymers because their degradation products are non-toxic metabolites that can be easily removed.

Polymer-based MPs for the treatment of tuberculosis (TB) have been extensively studied in vitro and in vivo. We demonstrated that PLGA MPs could effectively deliver an antitubercular medication into macrophages and maintain a greater intracellular concentration of the drug by controlled release, which suggests that the technology might be used to administer PLGA MP-based drug delivery [23]. In contrast to conventional medication, optimized moxifloxacin-PLGA-MPs were shown by Bhavya vishwa *et al.* to maintain drug residence in the lung for 24 hours following inhalation [24]. ISN and Rifabutin have been combined in one locust bean gum formulation for inhalable treatment of tuberculosis in the lungs by Susana Rodrigues *et al*. [25]. As prospective non-cytotoxic carriers for the pulmonary administration of INH, Oliveira *et al.* developed Chitosan MPs, which showed strong alveolar macrophage activation [26]. For diseases like tuberculosis (TB), where the pulmonary channel of infection is the natural route of infection, the increased interest by Margarida *et al.* in polymeric delivery methods for pulmonary administration of medications portends a more direct and efficient treatment approach. Drugs can be delivered directly to the lungs using polymeric microparticles or nanoparticles, and drug release can be controlled and sustained within TB-infected macrophages, enhancing anti-TB treatment efficacy and decreasing adverse effects [27].

In this study, we used hydrophobically modified starch propionate (SP) from starch as the drug carrier and formulation of ISN, RIF, and PYR drugs that could be encapsulated into starch propionate microparticles (SPMPs) by the oil-in-water (O/W) emulsion solvent evaporation method and investigated their chemical modification, morphology, crystallinity, thermal

behavior, and drug encapsulation efficiency with the help of FT-IR, FE-SEM, XRD, TG-DTA, and UV-Visible spectrophotometer, respectively. Besides, we also assessed their in vitro release characteristics and drug release mechanism by the dialysis membrane method.

## 2. MATERIALS AND METHODS

### 2.1 Materials

Corn starch was purchased from pallav chemicals & solvent Pvt. Ltd, (Tarapur, Maharastra, India). Concentrated sulfuric acid obtained from ACS chemicals (Ahmedabad, Gujarat, India). Glacial acetic acid, propionic anhydride, polyvinyl alcohol (PVA), and tetrahydrofuran (THF) were purchased from Sisco Research Laboratories Pvt. Ltd. (Taloja, Maharastra, India). Isoniazid (ISN), Rifampicin (RIF), and Pyrazinamide (PYR) was purchased from research-lab fine chem industries (Mumbai, Maharastra, India).

### 2.2 Methods

#### 2.2.1 Propionylation of starch

SP was synthesized with minor modifications from the method described by Mei Li *et al.* Magnetic stirring was used to mix 5 g of starch with 40 ml of glacial acetic acid in a three-necked flask. Once a homogenous solution had been obtained, 20 ml of cold propionic anhydride was poured into the flask and stirred gently. A catalyst, sulfuric acid (98%), was added to the flask contents after 15 minutes of stirring. Three hours of reflux at 90°C were terminated with cold distilled water (5°C), followed by filtering, and then washed with ethanol, followed by drying at 50°C overnight [28]

#### 2.2.2 Formulation of microparticles

The oil in water (O/W) single emulsification solvent evaporation process was used to formulate the ATD-loaded SPMPs. Organic phase prepared with known amounts of SP polymer and ATD were typically added to THF, which was thoroughly agitated to ensure that all material was properly dissolved in the solvent THF. The organic phase solution (5 mL) was then added drop wise by syringe (1 mg/ml) into the aqueous solution (20 mL) containing 1 %w/v PVA in the presence of sonication for 10 minutes with an ultra-probe sonicator set to 20 % amplitude in continuous mode (Fisher Scientific Sonicator model 505, Pittsburgh, PA-USA). To evaporate the organic solvent, the produced oil in water (O/W) emulsion was gently stirred at room temperature overnight with a magnetic stirrer (Remi, India). The ATD loaded SPMPs suspension were centrifuged at 10,000 rpm for 10 minutes (Kubota-600, Japan) and rinsed twice with distilled water to remove the surfactant and unloaded drug. To obtain the fine powder of MPs, the ATD-loaded into SPMPs was freeze-dried. A similar method was used to formulate blank SPMPs [29].

#### 2.2.3 Characterization

*2.2.3.1 FT-IR analysis*

The starch, SP, and blank SPMPs samples, as well as the KBr, were all dried. The dried material (1 mg) and KBr (150 mg) were crushed and combined before being pressed into a film shape under 0.5 MPa pressure. An FT-IR instrument measured the wavelength between 400 and 4000 $cm^{-1}$ (Nicolet IS50, Thermofisher, USA). With 32 scans, spectra were acquired.

*2.2.3.2 Crystalline study*

In this experiment, an X-ray diffractometer (600-Miniflex Rigaku Tokyo, Japan) was used to examine the sample findings of X-ray powder diffraction performed at 30 kV and 2 mA using scan speed and duration time of 10.0 deg./min., a Cu-K radiation ( = 1.542) detector, and a graphite monochromator were employed. To acquire data, the powders were scanned using a continuous scan mode through the 2 range of 3-90°. Prior to analysis, the samples were equilibrated to a constant weight at room temperature.

*2.2.3.3 Thermal analysis*

The dried samples (10.0 mg) were thermo gravimetrically analyzed (TGA) with a TG-DTA equipment (Perkin Elmer TGA 4000). The temperature program was run at a heating rate of 10°C/min from 25°C (room temperature) to 600°C in a nitrogen atmosphere (30 mL/min).

*2.2.3.4 Surface morphology and particle size*

Using a FE-SEM (JEOL JSM 7100F) at a 10 kV accelerating voltage, the granule surface and shape of SP, blank SPMPs, and ATD-loaded SPMPs were examined. To avoid electrical charge collection under the electron beam, the dehydrated samples were sprinkled on double-stick tape glued to circular copper stubs, then coated with a thin coating (15 nm) of gold. Using the computer software ImageJ, the particle size was calculated from SEM images.

*2.2.3.5 Encapsulation efficiency (%EE)*

A total of 10 mg of ATD loaded into SPMPs were ground and dissolved in 20 mL of methanol for 5 minutes using a sonicator. The drug solution was filtered, and the drug concentration was measured with a UV-Visible spectrophotometer at 265nm, 475nm, and 269nm for ISN, RIF, and PYR, respectively, and the encapsulation efficiency was estimated using the equations below.

$$\% \text{ EE} = \frac{[\text{Drug}]\text{total} - [\text{Drug}]\text{supernant}}{[\text{Drug}]\text{total}} \quad \text{Eq. (1)}$$

*2.2.3.6 In vitro drug release study*

The dialysis bag diffusion method was used to examine the in-vitro drug release of ATD loaded with SPMPs formulations. ATD were loaded with SPMPs suspension (5 ml) and placed in a dialysis bag, which was subsequently placed in a beaker containing 100 ml of pH 7.4 phosphate buffer saline (PBS). Throughout the experiment, the beaker was put over a magnetic stirrer, and the temperature of the assembly was kept at 37°C. Throughout the experiment, the rpm was held constant at 100 rpm. At regular intervals, sample (2 ml) was removed and replaced with equivalent volumes of fresh pH 7.4 PBS. The samples were examined using a UV–Visible spectrophotometer at 265nm, 475nm, and 269nm for ISN, RIF, and PYR, respectively [29].

*2.2.3.7 Drug release kinetics*

In vitro drug release data from ATD loaded with SPMPs were fit to various kinetic models, such as zero order, first order, and so on. The in vitro release data was fitted to Higuchi's and Korsmeyer-Peppas' models to better understand the drug release process. The highest correlation coefficient ($R^2$) values were used to assess drug release kinetics and mechanism [30].

## 3.0 RESULT & DISSCUSION

### 3.1 FT-IR analysis

Figure 1 shows the FT-IR spectra of the native starch, SP, and SPMPs. In native starch, distinct polysaccharide bands were visible, including an O-H stretching band spanning 3566-3000 $cm^{-1}$, two overlapping bands centred at 2931 and 2897 $cm^{-1}$, a small band centred at 1242 $cm^{-1}$ that could be attributed to a $CH_2OH$ (side chain)-related mode and a C–O–H deformation mode, and highly overlapped bands in the 1200-1150 $cm^{-1}$ region that could be attributed to the skeleton mode vibrations, C-H and $CH_2$ deformation, and C-C stretching vibrations were found to be the primary absorption bands in the native starch FT-IR spectra at lower wave numbers. The O-H bending vibration of adsorbed water molecules was ascribed to the band at 1641 $cm^{-1}$ [31]. Esterification was confirmed by the presence of propionate group vibrations in SP's FT-IR spectra. The most significant signal was a carbonyl ester group (C=O) stretching at 1749 $cm^{-1}$.Esterification was also confirmed by the 1236 $cm^{-1}$ signal, which was attributable to the C-O-C stretching vibration of the ester groups introduced [32]. The peak intensity of SPMPs' FT-IR spectra decreased slightly, but no changes to their characteristic peaks were observed.

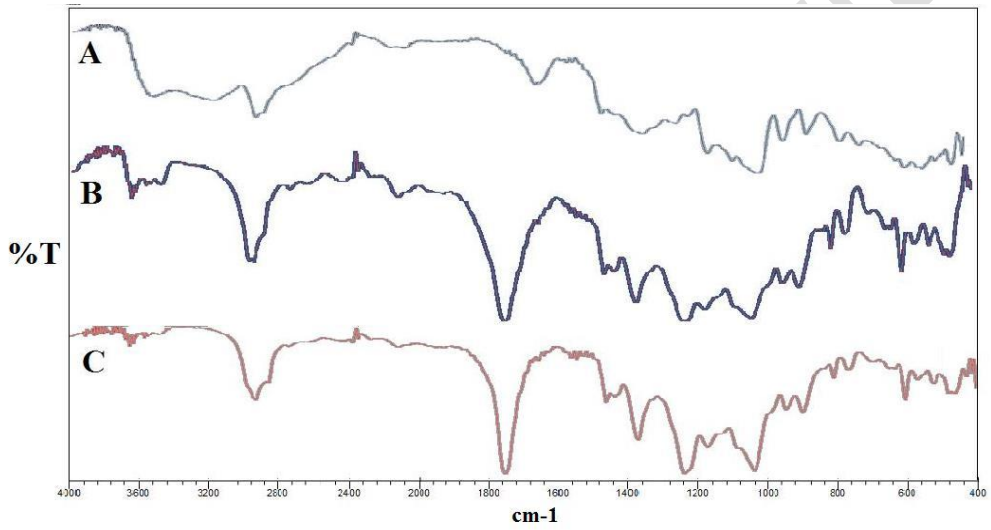


**Fig. 1.** FT-IR spectra of (A) native starch, (B) SP, and (C) SPMPs

### 3.2 Crystalline study

X-ray diffraction has been used to examine how propionylation at high DS levels affects starch's semi-crystalline structure. Figure 2(A) shows the native starch exhibited an A-type pattern, with reflections at 2θ: 15.30°, 17.11°, 19.97°, and 23°. Crystallinity loss during esterification has typically been attributed to an increase in hydrophobic ester groups substituting for starch hydroxyl groups that results in less inter- and intramolecular hydrogen bonding [33]. Figure 2(B) shows wide peak centred at 2θ = 20° appeared in the diffraction diagram of SP with high DS. According to previous studies, amorphous patterns have previously been seen in SP diffractograms, with typical wide peak areas around 6–9° and 20° (2θ) [34]. Figure 3(C) shows significant reduction in peak intensity was found for SPMPs derived from SP, when compared to that of SP. In high-intensity ultrasonication, the crystalline structure of SP is disrupted, resulting in SPMPs with low crystallinity or with an amorphous nature being formed.

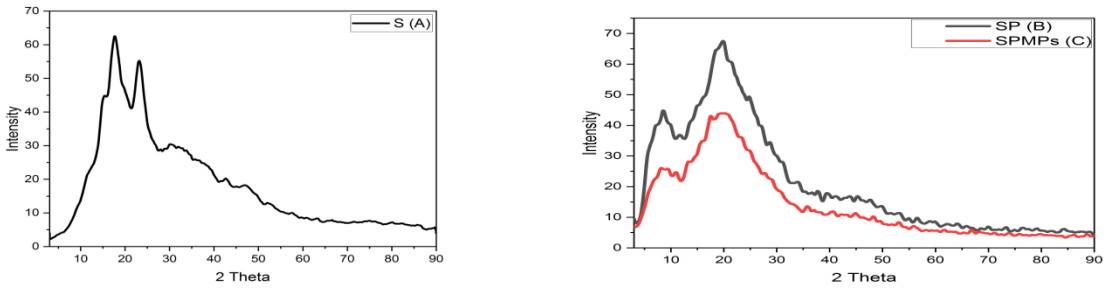


**Fig. 2.** X-ray diffraction patterns of (A) native starch, (B) SP, and (C) SPMPs

### 3.3 Thermal analysis

A thermal analysis study was performed to investigate the effect of propionylation on the starch's thermal characteristics. There were two stages in the weight loss of native starch: the first was a loss of water between 50°C and 115°C, with a weight loss of 11%. The native starch sample was stable up to 260°C after dehydration. Thermal breakdown resulted in a 75% weight loss when the temperature was raised from 260°C to 350°C (Fig. 3(A)). The predominant by-product of starch hydroxyl breakdown below 300°C was the generations of water through inter- or intramolecular condensation. There was only one stage to the weight loss for both SP and SPMPs, although the first stage weight loss from dehydration in SP and SPMPs was much less than in native starch due to their hydrophobicity. Decomposition temperatures in SP and SPMPs rose to 300–390°C and 300-386°C, respectively, with weight losses of 80%. Thus, it was evident from TG data that SP and SPMPs were thermally more stable than native starch and decomposition temperature increased. Compared to SP and SPMPs, DTG results showed that the rate of starch decomposition in native starch was higher than in SP and SPMPs (Fig. 3(B)). The reduced amount of hydroxyl groups in the modified starch molecule contributed to the improved thermal stability. The propionylation of hydroxyl groups, which increased the molecular weight and covalent bonding, was also responsible for the thermal stability. Because of its compact semi-crystalline structure, SP has better thermal stability than SPMPs [34].

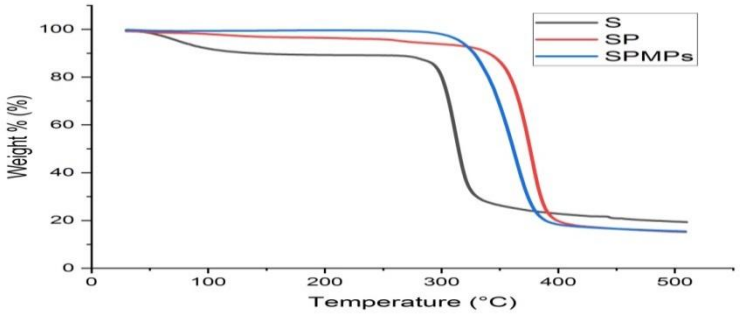


**Fig.3 (A).** TGA curves of native starches (S), starch propionate (SP), and starch propionate microparticles (SPMPs)

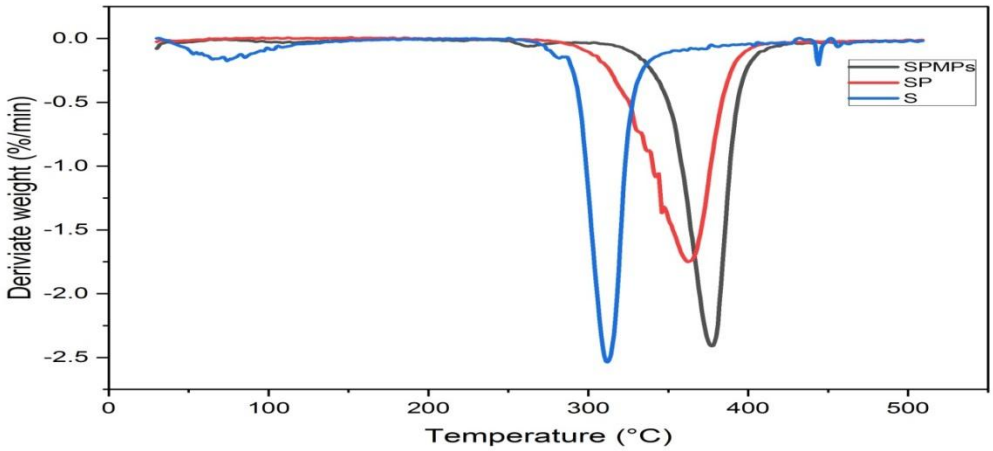


**Fig.3 (B).** DTG curves of native starch (S), starch propionate (SP), and starch propionate microparticles (SPMPs)

### 3.5 Surface morphology and particle size

In Figure 4, FE-SEM images of SPMPs (A, B), ISN loaded SPMPs (C, D), RIF loaded SPMPs (E, F), PYR loaded SPMPs (G, H), and SP (I, J) are shown. As demonstrated in Figures 4(I) and (J), After propionylation it was found that the starch's surface became rough and degraded, which was attributed to the replacement of propionate groups in the starch. Starch's granular structure was destroyed. Because of the increased surface area available for bonding and mechanical interlocking, starch with a rougher surface may have better adhesion to synthetic polymers. The starch granules start to rupture and different sizes of pores or cavities can be observed on the SP granules. The external as well as the internal part of the starch are seriously esterified and more pores and cavities are formed on the SP granules [34]. The size of SPMPs, ISN, RIF, and PYR loaded SPMPs were determined using FE-SEM and ImageJ software resulting in a geometric particle size of 1.243 ± 0.3 μm, 1.65 ± 0.2 μm, 2.73 ± 0.7 μm and 2.69 ± 0.5 μm respectively. As shown in the FE-SEM images, there were dimples and/or pores on the surface and in the bulk of the particles because the spontaneous w/o emulsion droplets acted as porogens [35].

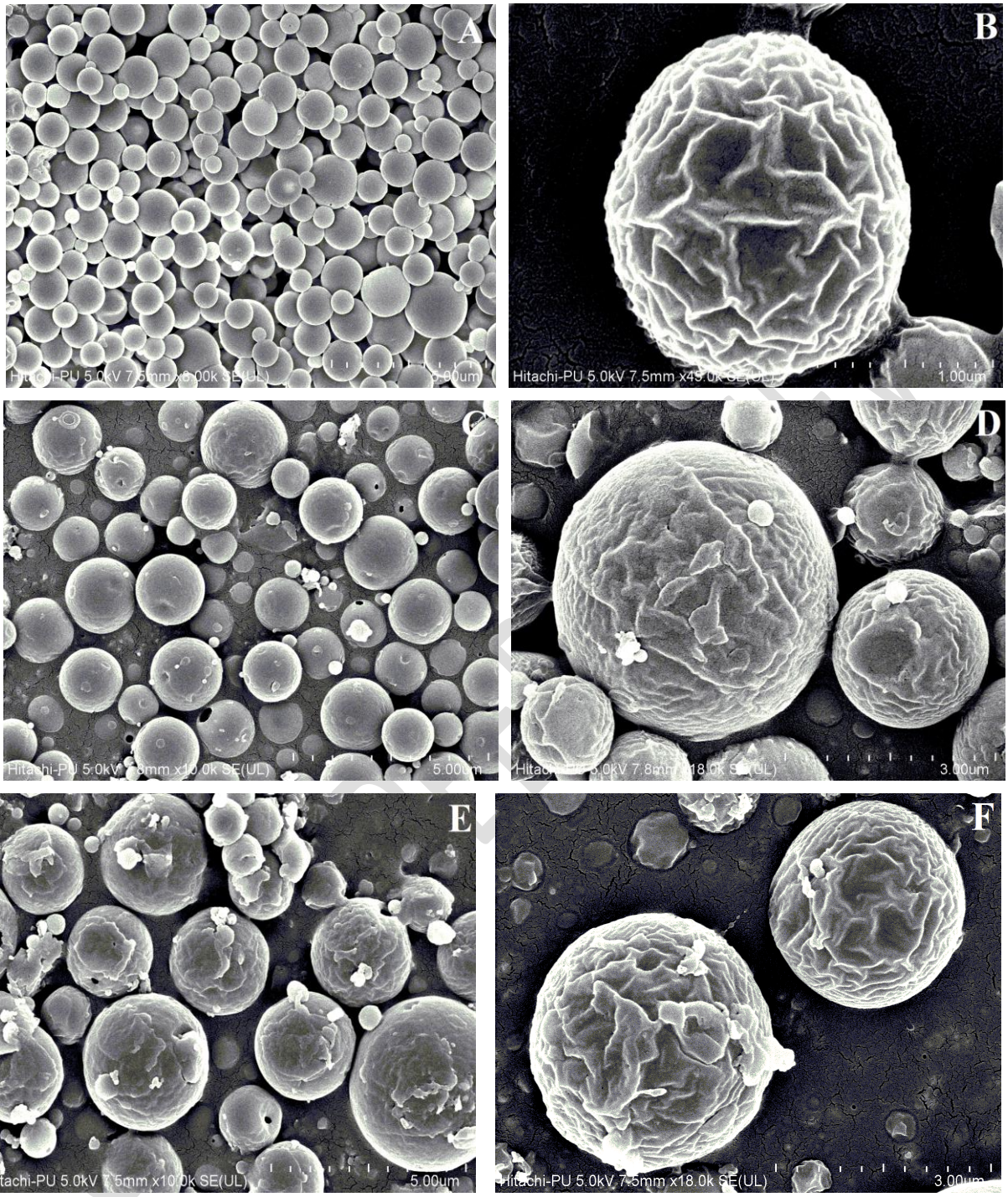
A
B
Hitachi-PU 5.0kV 7.5mm x45.0k SE(UL)
1.00um
C
Hitachi-PU 5.0kV 7.8mm x10.0k SE(UL)
5.00um
D
3.00um
E
Hitachi-PU 5.0kV 7.5mm x10.0k SE(UL)
5.00um
F
Hitachi-PU 5.0kV 7.5mm x18.0k SE(UL)
3.00um

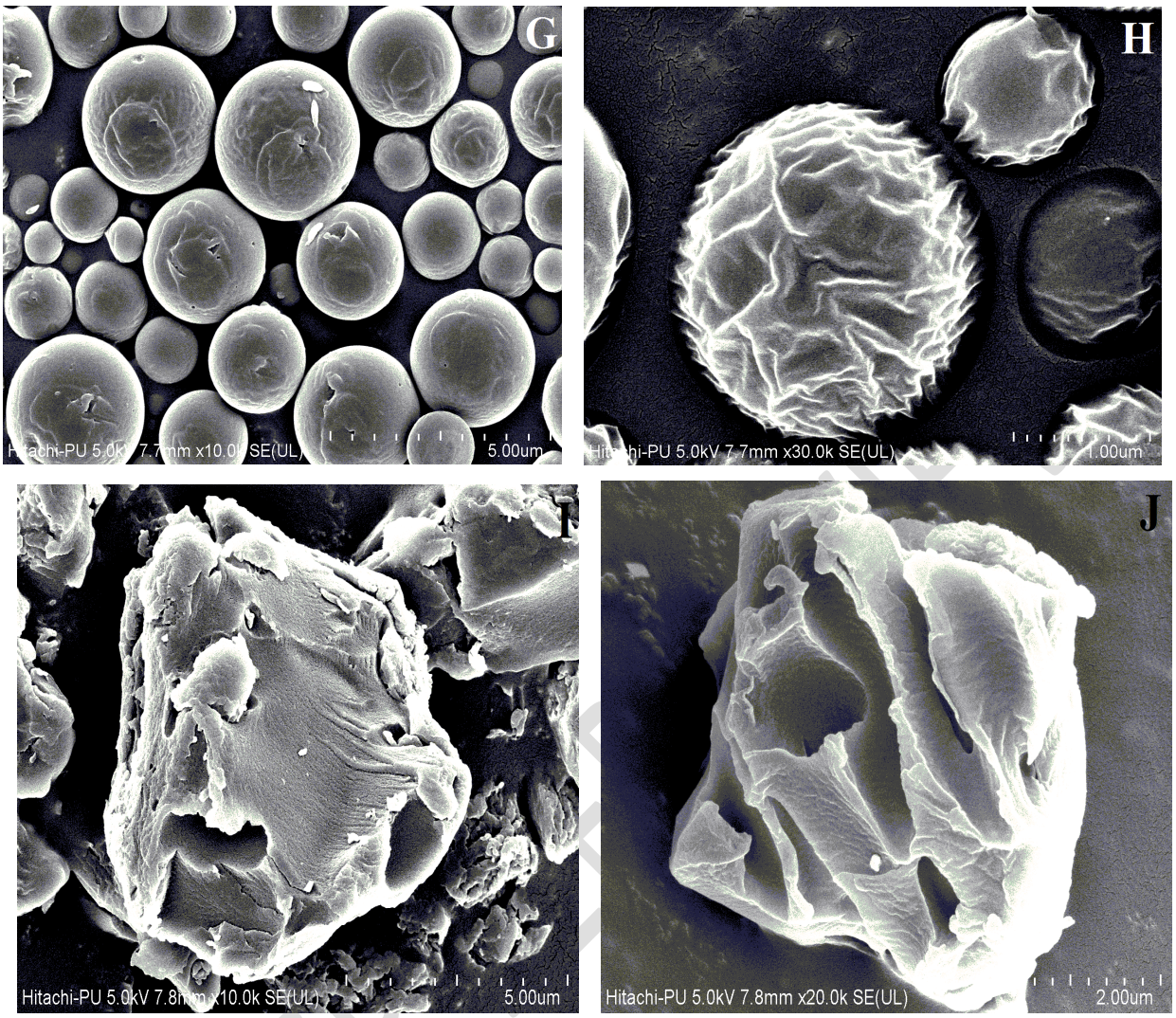


**Fig. (4).** FE-SEM images of (A, B) blank SPMPs, (C, D) ISN loaded SPMPs, (E, F) RIF loaded SPMPs, and (G, H) PYR loaded SPMPs and (I, J) SP

### 3.6 Encapsulation efficiency (%EE)

In considerations of formulation and large-scale production, encapsulation efficiency is a significant feature. Table 1 shows the %EE responses. Optimized formulation 1 had an ISN, RIF, and PYZ %EE of 37.6, 45.2, and 43.1, respectively. ISN, RIF, and PYR hydrophilic drugs may have had a weak interaction with the hydrophobic SP polymer, resulting in a lower %EE. Table 1 demonstrates the impact of the polymer to drug ratio on %EE for formulations 1, 2 and 3. Because sufficient polymer is needed to completely entrap the drug during the precipitation procedure and higher polymer concentration results in higher viscosity and, consequently, less partition of the drug into the external aqueous phase, a higher polymer to drug ratio (a ratio of 3:1) has a higher %EE value. Furthermore, formulations 3, 4, and 5 investigated the lower amount of drugs (a ratio of 1:3) that gave rise to a decrease in the layer thickness of the MPs. Apparently, it may contribute to the leakage of the drug, resulting in the lower E.E. value (Table 1, F 5) [36].

**Table1.** Encapsulation efficiency of ISN, RIF, and PYZ loaded SPMPs

| Formulation | Polymer to drug ratio | Isoniazid (%EE) | Rifampicin (%EE) | Pyrazinamid (%EE) |
|---|---|---|---|---|
| 1 | 3:1 | 37.6 | 45.2 | 43.1 |
| 2 | 2:1 | 35.7 | 38.1 | 35.9 |
| 3 | 1:1 | 21.2 | 33.7 | 25.7 |
| 4 | 1:2 | 18.2 | 30.2 | 23.1 |
| 5 | 1:3 | 16.2 | 25.6 | 24.8 |

### 3.6 In vitro drug release study

*In vitro* drug release from ATD loaded SPMPs and pure ATD were evaluated in PBS (pH 7.4) by modified dialysis bag diffusion method. During the initial 1 h of dissolution study, the pure ATD showed cumulative release of INH, RIF and PYZ in PBS (pH 7.4) as 96.1%, 90%, and 94.3% respectively. The release study of ATD loaded SPMPs formulation showed cumulative release of INH, RIF and PYZ in PBS (pH 7.4) as 20.4%, 14.2% and 19.1% respectively during initial 1 h. The pure ATD showed cumulative drug release of INH, RIF and PYZ in PBS (pH 7.4) more than 99% in 2 h, respectively. After 6 h, ATD loaded SPMPs formulation showed cumulative release of INH, RIF and PYZ in PBS (pH 7.4) as 60.2%, 50.8% and 57.8% respectively. ATD loaded SPMPs formulation showed cumulative release of INH, RIF and PYZ in PBS (pH 7.4) as 82.4%, 71% and 77.1% respectively during initial 12 h [37].

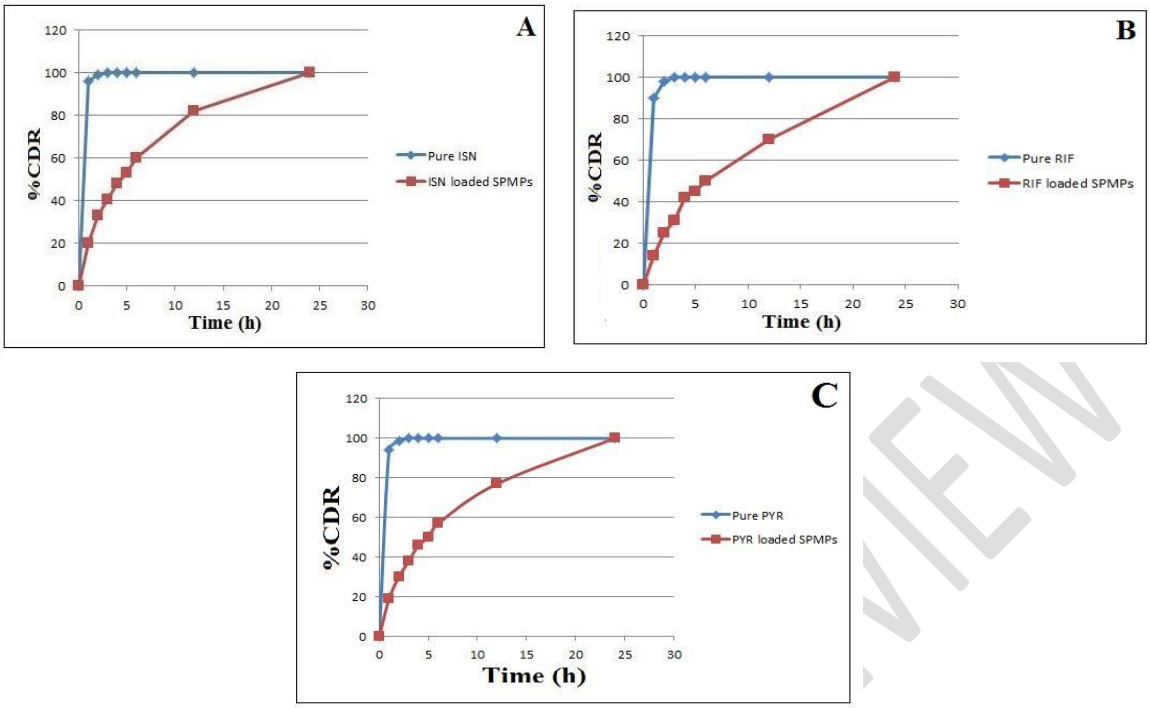


**Fig. (5).** In vitro percentage of cumulative drug release (%CDR) profile (A) Pure ISN and ISN loaded SPMPs, (B) Pure RIF and RIF loaded SPMPs, and (C) Pure PYR and PYR loaded SPMPs.

### 3.7 Drug release kinetics

The *in vitro* drug release data was fitted to different mathematical models such as zero order, first order, Higuchi's and Korsmeyer-Peppas' models. The regression linear *i.e.* squared correlation coefficient ($R^2$) was determined for each mathematical model (Table 2). Korsmeyer-Peppas' model showed the highest $R^2$ value for *in vitro* release of ISN, RIF and PYR loaded SPMPs were 0.9873, 0.9938 and 0.9928 respectively. The values of $0.45 < n < 0.89$ in Korsmeyer-Peppas' model indicates drug release by anomalous diffusion *i.e.*, non-Fickian diffusion [45, 46]. In the present study, the slope (n) value for *in vitro* release of ISN, RIF, and PYZ were 0.452, 0.539 and 0.467, respectively. Thus, the ATD release from SPMPs followed anomalous diffusion mechanism. However, the highest $R^2$ value for Korsmeyer-Peppas' model indicates the release mechanism followed diffusion controlled [38].

**Table 2.** Squared correlation coefficient ($R^2$) of different kinetic model**.**

| Release model | | ISN loaded SPMPs | RIF loaded SPMPs | PYR loaded SPMPs |
|---|---|---|---|---|
| Zero order | $R^2$ | 0.3760 | 0.6734 | 0.4742 |
| First order | $R^2$ | 0.9848 | 0.9848 | 0.9852 |

| | | | | |
|---|---|---|---|---|
| Higuchi's model | $R^2$ | 0.9771 | 0.9903 | 0.9898 |
| Korsmeyer - Peppas' model | $R^2$ | 0.9873 | 0.9938 | 0.9928 |

## 4. CONCLUSION

We have successfully developed ATD-loaded SPMPs for use as promising and biodegradable delivery methods to improve the efficacy of first-line ATD such as ISN, RIF, and PYR. FTIR, UV–Vis, FESEM, TGA, and XRD were used to investigate the experimental compounds' structural and morphological characteristics, thermal stability, and crystalline quality. In summary, native starch and SP has distinct structural and thermal properties. The emulsification solvent evaporation process produced ATD loaded SPMPs. ISN, RIF, and PYR loaded SPMPs had geometric particle sizes of 1.243 ± 0.3 μm, 1.65 ± 0.2 μm, 2.73 ± 0.7 μm and 2.69 ± 0.5 μm, respectively. In addition to dimples and/or pores on the surface of the spherical SPMPs, because the spontaneous emulsion droplets acted as porogens, the propionylation disrupted the morphological structure of the original starch granules. This is confirmed by FTIR. On the other hand, the ultrasonication impact on SPMPs results in lower crystallinity than SP. With increasing decomposition temperature, TGA showed SP and SPMPs to be thermally stable. ATD encapsulation efficiency on SPMPs ranged from 16-45%. During the first 12 hours, the CDR of INH, RIF, and PYZ in PBS (pH 7.4) was 82.4 percent, 71%, and 77.1 percent, respectively. We concluded that all improved formulations had controlled and sustained medication release over time. The model by Korsmeyer-Peppas has the highest $R^2$, indicating drug release by non-Fickian diffusion. The ATD loaded SPMPs may be a possible therapeutic strategy for tuberculosis.

COMPETING INTERESTS DISCLAIMER:

Authors have declared that no competing interests exist. The products used for this research are commonly and predominantly use products in our area of research and country. There is absolutely no conflict of interest between the authors and producers of the products because we do not intend to use these products as an avenue for any litigation but for the advancement of knowledge. Also, the research was not funded by the producing company rather it was funded by personal efforts of the authors.



## REFERANCES

1. Dua K, Rapalli VK, Shukla SD, Singhvi G, Shastri MD, Chellappan DK, Satija S, Mehta M, Gulati M, Pinto TD, Gupta G. Multi-drug resistant Mycobacterium tuberculosis &

oxidative stress complexity: emerging need for novel drug delivery approaches. Biomedicine & Pharmacotherapy. 2018 Nov 1;107:1218-29.
2. WHO. Tuberculosis. 2021.
3. Gajendiran M, Gopi V, Elangovan V, Murali RV, Balasubramanian S. Isoniazid loaded core shell nanoparticles derived from PLGA–PEG–PLGA tri-block copolymers: in vitro and in vivo drug release. Colloids and Surfaces B: Biointerfaces. 2013 Apr 1;104:107-15.
4. Adepu, Shivakalyani, and Seeram Ramakrishna. "Controlled Drug Delivery Systems: Current Status and Future Directions." *Molecules* 26, no. 19 (2021): 5905.
5. Navalakhe RM, Nandedkar TD. Application of nanotechnology in biomedicine.
6. Shastri MD, Shukla SD, Chong WC, Dua K, Peterson GM, Patel RP, Hansbro PM, Eri R, O'Toole RF. Role of oxidative stress in the pathology and management of human tuberculosis. Oxidative medicine and cellular longevity. 2018 Oct 11;2018.
7. Koch A, Cox H, Mizrahi V. Drug-resistant tuberculosis: challenges and opportunities for diagnosis and treatment. Current Opinion in pharmacology. 2018 Oct 1;42:7-15.
8. Nasiruddin M, Neyaz M, Das S. Nanotechnology-based approach in tuberculosis treatment. Tuberculosis research and treatment. 2017 Jan 22;2017.
9. Lagreca E, Onesto V, Di Natale C, La Manna S, Netti PA, Vecchione R. Recent advances in the formulation of PLGA microparticles for controlled drug delivery. Progress in Biomaterials. 2020 Oct 15:1-22.
10. Chung CH, Cui B, Song R, Liu X, Xu X, Yao S. Scalable production of monodisperse functional microspheres by multilayer parallelization of high aspect ratio microfluidic channels. Micromachines. 2019 Sep;10(9):592.
11. Ospina-Villa JD, Gómez-Hoyos C, Zuluaga-Gallego R, Triana-Chávez O. Encapsulation of proteins from Leishmania panamensis into PLGA particles by a single emulsion-solvent evaporation method. Journal of microbiological methods. 2019 Jul 1;162:1-7.
12. McKiernan PJ, Lynch P, Ramsey JM, Cryan SA, Greene CM. Knockdown of gene expression in macrophages by microRNA mimic-containing poly (lactic-co-glycolic acid) microparticles. Medicines. 2018 Dec;5(4):133.
13. Choi YS, Joo JR, Hong A, Park JS. Development of drug-loaded PLGA microparticles with different release patterns for prolonged drug delivery. Bulletin of the Korean Chemical Society. 2011;32(3):867-72.
14. Guo W, Quan P, Fang L, Cun D, Yang M. Sustained release donepezil loaded PLGA microspheres for injection: Preparation, in vitro and in vivo study. asian journal of pharmaceutical sciences. 2015 Oct 1;10(5):405-14.
15. Takeuchi I, Tomoda K, Hamano A, Makino K. Effects of physicochemical properties of poly (lactide-co-glycolide) on drug release behavior of hydrophobic drug-loaded nanoparticles. Colloids and Surfaces A: Physicochemical and Engineering Aspects. 2017 May 5;520:771-8.
16. Takeuchi I, Tomoda K, Hamano A, Makino K. Effects of physicochemical properties of poly (lactide-co-glycolide) on drug release behavior of hydrophobic drug-loaded nanoparticles. Colloids and Surfaces A: Physicochemical and Engineering Aspects. 2017 May 5;520:771-8.
17. Strobel SA, Hudnall K, Arbaugh B, Cunniffe JC, Scher HB, Jeoh T. Stability of fish oil in calcium alginate microcapsules cross-linked by in situ internal gelation during spray drying. Food and Bioprocess Technology. 2020 Feb;13(2):275-87.

18. Shah NK, Wang Z, Gupta SK, Le Campion A, Meenach SA. Sustained release of a model water-soluble compound via dry powder aerosolizable acetalated dextran microparticles. Pharmaceutical development and technology. 2019 Oct 21;24(9):1133-43.
19. Batista P, Castro P, Madureira AR, Sarmento B, Pintado M. Development and characterization of chitosan microparticles-in-films for buccal delivery of bioactive peptides. Pharmaceuticals. 2019 Mar;12(1):32.
20. da Silva MT, Pinto JC. Influence of encapsulated aroma compounds on the formation and morphology of gelatin microparticles. InMacromolecular Symposia 2019 Feb (Vol. 383, No. 1, p. 1800061).
21. Farrag Y, Malmir S, Montero B, Rico M, Rodríguez-Llamazares S, Barral L, Bouza R. Starch edible films loaded with donut-shaped starch microparticles. LWT. 2018 Dec 1;98:62-8.
22. Makadia HK, Siegel SJ. Poly lactic-co-glycolic acid (PLGA) as biodegradable controlled drug delivery carrier. Polymers. 2011 Sep;3(3):1377-97.
23. Liu Z, Li X, Xiu B, Duan C, Li J, Zhang X, Yang X, Dai W, Johnson H, Zhang H, Feng X. A novel and simple preparative method for uniform-sized PLGA microspheres: preliminary application in antitubercular drug delivery. Colloids and Surfaces B: Biointerfaces. 2016 Sep 1;145:679-87.
24. Vishwa B, Moin A, Gowda DV, Rizvi S, Hegazy WA, Abu Lila AS, Khafagy ES, Allam AN. Pulmonary Targeting of Inhalable Moxifloxacin Microspheres for Effective Management of Tuberculosis. Pharmaceutics. 2021 Jan;13(1):79.
25. Rodrigues S, Alves AD, Cavaco JS, Pontes JF, Guerreiro F, da Costa AM, Buttini F, Grenha A. Dual antibiotherapy of tuberculosis mediated by inhalable locust bean gum microparticles. International journal of pharmaceutics. 2017 Aug 30;529(1-2):433-41.
26. Oliveira PM, Matos BN, Pereira PA, Gratieri T, Faccioli LH, Cunha-Filho MS, Gelfuso GM. Microparticles prepared with 50–190 kDa chitosan as promising non-toxic carriers for pulmonary delivery of isoniazid. Carbohydrate polymers. 2017 Oct 15;174:421-31.
27. Miranda MS, Rodrigues MT, Domingues RM, Torrado E, Reis RL, Pedrosa J, Gomes ME. Exploring inhalable polymeric dry powders for anti-tuberculosis drug delivery. Materials Science and Engineering: C. 2018 Dec 1;93:1090-103.
28. Li M, Wang F, Wang J, Wang R, Strappe P, Zheng B, Zhou Z, Chen L. Manipulation of the internal structure of starch by propionyl treatment and its diverse influence on digestion and in vitro fermentation characteristics. Carbohydrate Polymers. 2021 Oct 15;270:118390.
29. Bohrey S, Chourasiya V, Pandey A. Polymeric nanoparticles containing diazepam: preparation, optimization, characterization, in-vitro drug release and release kinetic study. Nano Convergence. 2016 Dec;3(1):1-7.
30. Khatak S, Mehta M, Awasthi R, Paudel KR, Singh SK, Gulati M, Hansbro NG, Hansbro PM, Dua K, Dureja H. Solid lipid nanoparticles containing anti-tubercular drugs attenuate the Mycobacterium marinum infection. Tuberculosis. 2020 Dec 1;125:102008.
31. Hampe R, Heinze T. Studies about the solvent-dependent substitution pattern of starch acetates. Macromolecular Materials and Engineering. 2014 Oct;299(10):1188-96.
32. Di Filippo S, Tupa MV, Vázquez A, Foresti ML. Organocatalytic route for the synthesis of propionylated starch. Carbohydrate polymers. 2016 Feb 10;137:198-206.
33. Diop CI, Li HL, Xie BJ, Shi J. Effects of acetic acid/acetic anhydride ratios on the properties of corn starch acetates. Food chemistry. 2011 Jun 15;126(4):1662-9.

34. Garg S, Jana AK. Characterization and evaluation of acylated starch with different acyl groups and degrees of substitution. Carbohydrate Polymers. 2011 Feb 1;83(4):1623-30.
35. Nishimura S, Murakami Y. Precise Control of the Surface and Internal Morphologies of Porous Particles Prepared Using a Spontaneous Emulsification Method. Langmuir. 2021 Mar 3;37(10):3075-85.
36. Qiu C, Hu Y, Jin Z, McClements DJ, Qin Y, Xu X, Wang J. A review of green techniques for the synthesis of size-controlled starch-based nanoparticles and their applications as nanodelivery systems. Trends in Food Science & Technology. 2019 Oct 1;92:138-51.
37. Khatak S, Mehta M, Awasthi R, Paudel KR, Singh SK, Gulati M, Hansbro NG, Hansbro PM, Dua K, Dureja H. Solid lipid nanoparticles containing anti-tubercular drugs attenuate the Mycobacterium marinum infection. Tuberculosis. 2020 Dec 1;125:102008.
38. Bohrey S, Chourasiya V, Pandey A. Polymeric nanoparticles containing diazepam: preparation, optimization, characterization, in-vitro drug release and release kinetic study. Nano Convergence. 2016 Dec;3(1):1-7.